ACS APPLIED MATERIALS & INTERFACES

Energy, Environmental, and Catalysis Applications

High Performance Zinc-Air Battery with Scalable Metal-Organic Framework and Platinum Carbon Black Bifunctional Catalyst

Juntao Li, Zhu Meng, Dan J.L. Brett, Paul R Shearing, Neal T. Skipper, Ivan P. Parkin, and Srinivas Gadipelli

ACS Appl. Mater. Interfaces, **Just Accepted Manuscript** • DOI: 10.1021/acsami.0c10151 • Publication Date (Web): 27 Aug 2020

Just Accepted

is published by the American Chemical Society. 1155 Sixteenth Street N.W., Washington, DC 20036

High Performance Zinc-Air Battery with Scalable Metal-Organic Framework and Platinum Carbon Black Bifunctional Catalyst

Juntao Li, Zhu Meng, Dan J. L. Brett, Paul Shearing, Neal T. Skipper, Ivan P. Parkin, and Srinivas Gadipelli*

AUTHOR ADDRESS

Juntao Li, Prof. Ivan P. Parkin. Department of Chemistry, University College London, London, WC1H 0AJ, United Kingdom

Zhu Meng. Molecular Sciences Research Hub, Imperial College London, London, W12 0BZ, United Kingdom

Prof. Dan J. L. Brett, Prof. Paul Shearing, Dr. Srinivas Gadipelli. Electrochemical Innovation Lab, Department of Chemical Engineering, University College London, London, WC1E 7JE, United Kingdom

Prof. Dan J. L. Brett, Prof. Paul Shearing. The Faraday Institution, Quad One, Harwell Science and Innovation Campus, Didcot, OX11 0RA, United Kingdom

Prof. Neal T. Skipper. Department of Physics & Astronomy, University College London, London WC1E 6BT, United Kingdom

KEYWORDS: metal-organic framework, zinc-air battery, zeolitic-imidazolate framework, platinum carbon black, bifunctional catalysis

ABSTRACT: Metal-organic frameworks (MOFs) related derivatives have generated significant interest in numerous energy conversion and storage applications, such as adsorption, catalysis and batteries. However, such materials real world applicability is hindered due to scalability and reproducibility issues as they are produced by multistep post-synthesis modification of MOFs, often with high temperature carbonization and/or calcination. In this process, MOFs act as self-sacrificial templates to develop functional materials at the expense of sever mass-loss and the resultant materials exhibits complex process-performance relationships. In this work, we report direct applicability of readily synthesized and commercially available MOF, zeolitic imidazolate framework (ZIF-8) in a rechargeable zinc-air battery. The composite of cobalt based ZIF-8 and platinum carbon black (ZIF-67@Pt/CB) prepared via facile solution mixing shows a promising bifunctional electrocatalytic activity for oxygen evolution and reduction reactions (OER and ORR), the key charge and discharge mechanisms in a battery. ZIF-67@Pt/CB exhibits long OER/ORR activity durability, notably, a significantly enhanced ORR stability compared to Pt/CB; 85% vs 52%. Interestingly, ZIF-67@Pt/CB based battery delivers high performance with power density of >150 mW cm^{-2} and long stability for 100 h charge-discharge cyclic test run. Such remarkable activities from as-produced ZIF-67 is attributed to the electrochemically driven in-situ development of active cobalt-(oxy)hydroxide nanophase and interfacial interaction with platinum nanoparticles. This work shows commercial feasibility of zinc-air batteries as MOF-cathode materials can be reproducibly synthesized in mass scale and applied as produced.

Introduction

Aqueous rechargeable zinc-air battery, a promising next generation electrochemical energy storage system, has great advantages in terms of high energy density and excellent safety.[1-3] The battery basically operates with oxygen catalysis reactions, oxygen evolution reaction (OER) and oxygen reduction reaction (ORR) that occur at the air electrode with catalyst layer. The noble metal nanoparticles, e.g. the platinum group metals, Pt and Ru/Ir (PGM) are key electrocatalyst materials for ORR and OER, respectively. Thus, a low cost, scalable and high performing alternative bifunctional catalyst material is essential for commercialization of the battery technology. For example, the mass scale applicability of platinum (normally 20 % or 40 % on carbon black; Pt/CB) is hindered due to the low abundance and subsequent high cost, and associated performance issues of low mass activity, poor rechargeable efficiency and short cycle life.[1-6] Therefore, numerous materials families have been actively investigated, which include more widely metals/alloys, carbons and organic frameworks based nanostructures.[1-10]The efforts also include improving the main bottleneck issues of PGM catalysts via alloying or combining with earth abundant transition metals and porous organic/inorganic substrate materials to enhance their mass activity and durability at a greatly reduced amount of mass loading.[5,6,11-13] As the OER/ORR proceeds via adsorption/conversion of gaseous/liquid phase reactants and products at a triple phase boundary of solid-liquid-gas interface involving catalyst-electrolyte-oxygen, the porous solids with high specific surface area and electrical conductivity are most suitable candidate catalyst support materials.[1-13] Such structures can be tailored with rational creation of heterogeneous surface (a binding site density,

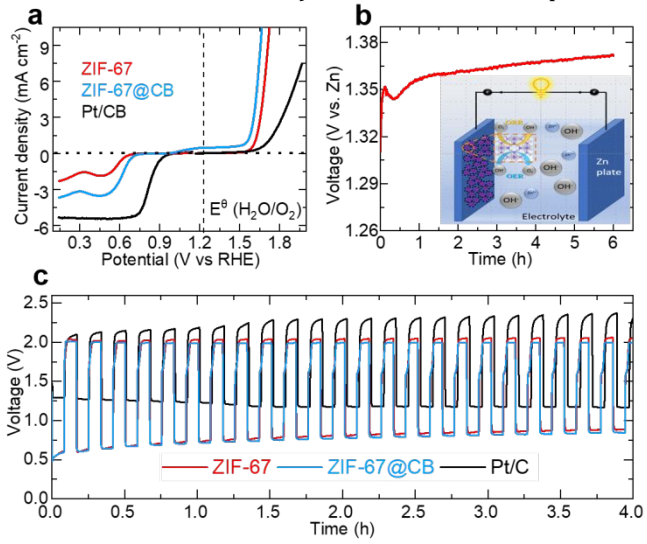

Figure 1. Initial electrochemical activity assessment of ZIF-67 with reference Pt/CB: a) Combined ORR and OER LSV curves of ZIF-67, ZIF-67@CB and Pt/CB. All the measurements were carried out in a 0.1 M KOH electrolyte in three electrode configuration with rotating disk electrode method at 1600 rpm. **b)** OCV of a zinc-air battery with ZIF-67 catalyst deposited on the gas diffusion layer carbon paper (GDLCP) as cathode, with inset for schematic representation of a zinc-air battery cell. **c)** Charge-discharge cyclic tests of batteries made with different catalysts deposited on GDLCP as cathode and operated at a fixed current density of 5 mA cm^{-2}.

with defects and dopants) and active centers (a catalyst site density, with nanoparticles of metals, alloys, oxides and combinations) to promote the adsorption/conversion of catalytic reactions.[1-17] The metal-organic frameworks (MOFs), intrinsically porous structures formed with earth-abundant transition metal node and organic linker units, can satisfy the desirable catalytic properties involving adsorption-conversion-distribution simultaneously.[8,10,12-23] Indeed, MOFs as well as their related derivatives have shown great promise for wide range of energy storage and conversion applications, including molecular, liquid/gas/vapor adsorption and chemical catalytic conversions. Moreover, MOFs often exhibit extremely high and widely tunable internal surface area, pore geometry and surface/interface chemistry along with external nano/microstructure to offer rich binding and catalytic site density. The MOF derivatives are often oxides and carbon structures, developed from high temperature thermolysis of MOFs as sacrificial templates. For example, carbonization of MOFs involves severe decomposition of the linker organic ligand and leads to a very low-level mass yield of catalyst, (10–20) wt%,[8,14,24-26] and poses significant challenges for controlling composition, functionality, porosity and nanophase, as well as for mass production. Further to this, as each type of precursor MOFs exhibits different strengths of framework thermal stability, metal-ligand coordination, pore structure, and ligand functionality, it is difficult to design and standardize the thermolysis parameters to achieve a desirable carbon structure. Thus the carbon-based electrocatalysts show very complex structure-performance relationships, which are directly attributed to the lack of reproducibility and fine control over the carbonization of MOFs.[10,18,19,22,27,28] Hence, utilizing MOFs directly maybe ideal for the electrochemically driven catalytic conversions, as they can be reproducibly synthesized, well characterized and prepared in large scale.[27,28] Here it is worth noting that the poor electrical conductivity of MOFs is a major limiting factor.[14,22,29,30] Recent studies show that the as-prepared MOFs, without carrying out thermolysis, are actively explored for OER and metal-air battery applications.[10,18,19] However there are very few instances MOFs are applied directly in aqueous zinc-air battery compared to organic lithium-air battery.

In this work, for the first time, we show that the readily available MOF, a zeolitic imidazolate framework (ZIF-8) can be easily turned into a high performing zinc-air battery cathode material. For example, ZIF-8 based structures, including its cobalt analogue, ZIF-67 or bimetallic ZIF-8, can be produced quickly and in large quantities,[24,27,28] and are also commercially produced and supplied by BASF under the trade name of Basolite® Z1200. Briefly, both ZIF-8 and ZIF-67 in gram scale were synthesized at room temperature stirring from methanol solvent and used directly for battery and other electrochemical and structural characterizations without further chemical modifications, such as high temperature calcination/carbonization, usually performed in the literature. As shown in **Figure 1,** the initial tests on ZIF-67 sample suggest a promising OER activity and battery performance, particularly the encouraging level of open circuit voltage (OCV) value and low voltage value for a charge step during the charge-discharge cycles. Worth noting that such activities in ZIF-67 are further improved with the addition of conducting carbon black (ZIF-67@CB). However, it can be seen that the ORR activity, and associated discharge step from ZIF-67 is very poor compared to Pt/CB reference catalyst. Here it is important to note a relatively poor OER activity or high voltage charge step from Pt/CB. Considering with these activities, we develop a highly efficient bifunctional catalyst, by simply combining ZIF-67 and Pt/CB (ZIF-67@Pt/CB) via facile solution casting route, that delivers excellent bifunctional oxygen catalytic activity and battery performance with small voltage difference between charge-discharge cycles, high peak power density, impressive energy density, and remarkable cycle life compared to the Pt/CB or combined Pt/CB+IrO_2 reference catalysts. Isostructural ZIF-8@Pt/CB is also synthesized and examined to understand the activity insights. Further analysis with post electrochemical examinations, for example, after 20 h ORR durability and 50 h battery charge-discharge cycling tests, indicate interfacial interaction between electrochemically driven in-situ formed highly active amorphous cobalt-hydroxide/oxyhydroxide nanosheets and platinum nanoparticles, which in turn improves bifunctional catalytic activity durability and battery cycle life.

Results and discussion

ZIF-67 sample, that exhibits high quality structure[14,24] is synthesized and used directly for the electrochemical examination without high temperature thermolysis, calcination or carbonization. Then ZIF-67@Pt/CB and ZIF-67@Pt/CB-2 catalysts in different mass ratios 1:1 and 2:1

of ZIF-67 and Pt/CB, respectively are prepared via simple solution mixing and casting route at room temperature (Scheme S1). For comparison, ZIF-8@Pt/CB is also prepared in a similar fashion. The sample preparation, the thin electrocatalyst layer deposition on the gas diffusion layer carbon paper (GDLCP) for a mass loading of 0.5 mg

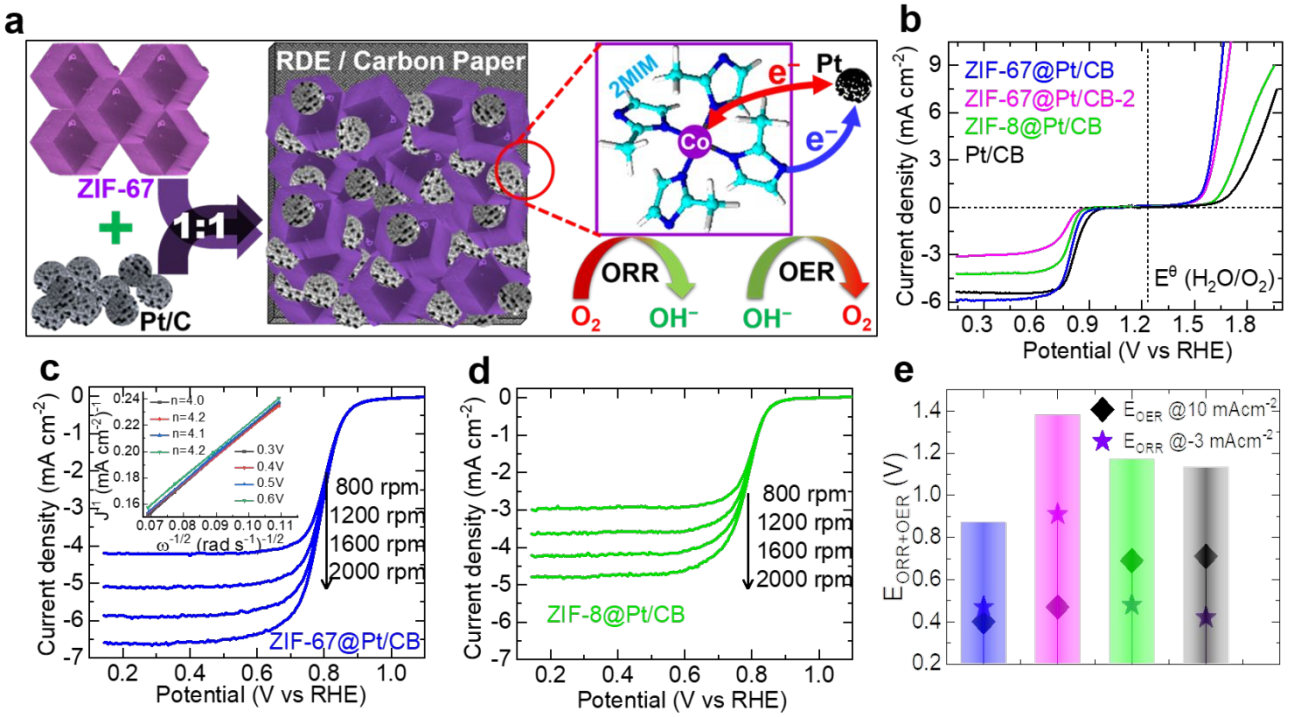

Figure 2. Bifunctional (for both OER and ORR) catalytic activity of ZIF-67@Pt/CB with reference ZIF-8@Pt/CB and Pt/CB samples: a) Preparation of catalysts via facile solution method at room temperature with insights for local framework structure/surface platinum interaction. **b)** Combined ORR and OER LSV curves of catalysts in 0.1 M KOH at 1600 rpm. **c-d)** ORR LSV curves of ZIF-67@Pt/CB and ZIF-8@Pt/CB at different rotating speeds, with inset for Koutechy-Levich plot linear fittings. **e)** Potential difference for bifunctional activity with respective ORR and OER overpotential values recorded at -3 and 10 mA cm^{-2}, respectively for studied catalysts. Same color code applies for the samples in all subpanel graphs.

cm^{-2} from aqueous dispersions with Nafion binder, is schematically presented in Figure 2a. The GDLCP coated with composite sample is directly used as cathode, an air electrode, to fabricate the battery with polished zinc foil as anode and aqueous KOH electrolyte. Before this, all the catalyst materials activity performance is assessed using rotating disc electrode (RDE) method (experimental details). As shown in Figure 2b, the linear sweep voltammetry (LSV) curves reveal a highly improved OER and ORR activity in ZIF-67@Pt/CB compared to ZIF-67@Pt/CB-2 (i.e., with 25 wt% of Pt/CB loading) and ZIF-67 (Figure 1a) or Pt/CB alone. The OER potential at current density of 10 mA cm^{-2} is reduced to 1.66 V (vs RHE) in ZIF-67@Pt/CB sample compared to 1.8 and >2.0 V (vs RHE) in ZIF-67 and Pt/CB, respectively. Interestingly, ZIF-67@Pt/CB also exhibits a comparable ORR activity to Pt/CB even with 50 wt% reduced Pt/CB loading. Moreover, Koutecky–Levich (K–L) and Tafel plots reveal 4 electron ORR activity pathway with enhanced kinetics in ZIF-67@Pt/CB sample, which is equivalent to the Pt/CB (Figure 2c and Figure S1 and S2).[24] Here it is worth noting that zinc based isostructural ZIF-8@Pt/CB sample do not show such improved catalytic activities, but a reduced ORR activity can be seen in terms of unfavorable onset and half-wave potentials with significantly reduced limiting current density as well as electron transfer number, ~2.6 (Figure 2d and Figure S1). The double layer capacitance (C_{dl}) of ZIF-67@Pt/CB is comparable to Pt/CB, whereas ZIF-67@Pt/CB-2 and ZIF-8@Pt/CB samples show reduced values (Figure S3). Electrochemical impedance spectroscopy (EIS) indicates an efficient electrolyte diffusion within ZIF-67@Pt/CB based electrode structure (Figure S4). It is important to note that among the samples, the ZIF-67@Pt/CB shows best bifunctional activity with a small potential difference of ~0.87 V between benchmark current densities of −3 mA cm^{-2} and 10 mA cm^{-2} for ORR and OER respectively (Figure 2e, Table S1). This value is considerably smaller than ~1.14 and ~1.17 V for Pt/CB and ZIF-8@Pt/CB respectively, but comparable to many other carbonaceous or metal-/metal-oxide based bifunctional catalysts reported in the literature (Figure S5 and Table S1).

The structural characterizations show that composite, ZIF-67@Pt/CB in the powder form remains highly porous with specific surface area of 1201 m^2 g^{-1} (Figure S6 and Table S2). The powder X-ray diffraction (XRD), porosity and CO_2 uptake data with Fourier transform infrared (FTIR) spectra, and scanning and transmission electron microscopy (SEM and TEM) images presented in Figure 3a-c (and Figure S6) indicates that the sample deposited on GDLCP retains its overall crystallinity, framework and morphology of ZIF-67. The SEM and TEM further shows the homogeneous distribution of Pt/CB at ZIF-67 surface,

which is supported by energy-dispersive X-ray spectroscopy (EDX) mapping images of ZIF-67@Pt/CB (Figure S7). It is interesting to note that XPS shows a clear chemical interaction between platinum and ZIF-67 structure with modified Co-N, Co-Pt and Pt-N bonds from the respective Pt 4f, Co 2p and N 1s peak shift to higher binding energy compared to Pt/CB and ZIF-67 (Figure 3d-f and Figure S8).[12,13,31] Lewis basic N- (nitrogen) groups of framework imidazolate act as electron donors and thus facilitate

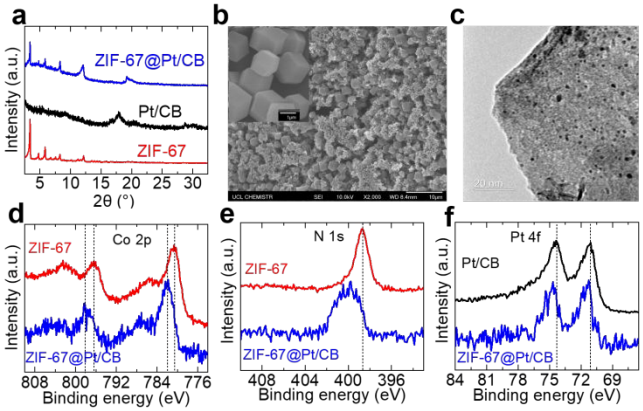

Figure 3. Structural characteristics of the catalyst samples deposited on GDLCP: a-c) XRD patterns (a) SEM (b) and TEM (c) of ZIF-67@Pt/CB sample. The parent ZIF-67 and Pt/CB powder samples XRD patterns are also provided (a), and inset of (b) shows a SEM of ZIF-67 powder sample. **d-f)** XPS core level spectra of Co 2p, N 1s and Pt 4f of ZIF-67@Pt/CB with respect to parent ZIF-67 and Pt/CB powder samples. The peak shifts to higher binding energy in ZIF-67@Pt/CB with respect to ZIF-67 or Pt/CB can be seen, for instance, Co 2p at 781.8 eV from 780.6 eV, N 1s at r 398.6 eV and Pt 4f at 71.4 eV from 71.1 eV.

strong surface interaction and fine dispersion of platinum nanoparticles over ZIF-67 particles, as supported with TEM and EDX (Figure 3c and Figure S7). Here worth noting that N 1s spectra of ZIF-67@Pt/CB shows relatively broad peak with two peaks at ~399.4 eV and ~400.8 eV and are assigned respectively to modified metal-nitrogen coordination and pyrrolic nitrogen due to introduction of Pt/CB and partially decomposition of ZIF-67 structure, respectively during the electrode preparation under sonication in aqueous and binder Nafion solution (Figure S8). The defect induced N 1s broadening and development of pyrrolic nitrogen is often observed when treated ZIF-67 or ZIF-8 structure under electrochemically in aqueous solution or under oxygen plasma or thermally oxidized under controlled conditions.[32-39]

Next, ZIF-67@Pt/CB sample catalytic performance is studied in a rechargeable zinc-air battery liquid cells, along with reference Pt/CB and Pt/CB+IrO_2 catalysts (Figure 4). As shown in Figure 4a, the ZIF-67@Pt/CB based battery produces an impressive and stable OCV of 1.42 V for 20 h. Figure 4b shows a comparative galvanodynamic charge/discharge polarization and corresponding discharge power density curves for ZIF-67@Pt/CB, which delivers a large current density of 100 mA cm^{-2} at a voltage of 1.0 V and maximum power density of >150 mW cm^{-2} at 300 mA cm^{-2}. These values are comparatively higher with respect to the Pt/CB and Pt/CB+IrO_2 based catalysts, which exhibit around 60 mA cm^{-2} and 90 mW cm^{-2}, respectively. The peak power density of over 150 mW cm^{-2} at 300 mA cm^{-2} in ZIF-67@Pt/CB is also high compared to many ZIF-derived nanocarbon and other catalyst materials reported in recent years (Figure S9 and Table S3 and S4). For instance, Co_3O_4@N-CNMAs/CC sample exhibits lower peak power density of around 75 mW cm^{-2} synthesized via multistep-precursor design, such as growing 3D ZIF-67 on 2D ZIF-L at carbon cloth, followed by two-step process of carbonization and oxidation.[40] In another instance, GNCNTs reaches a power density of 150 mW cm^{-2}, which is designed by multi-step growth of ZIF-67 on graphene oxide then carbonization at 700 °C followed by H_2SO_4 washing residual cobalt.[41] Co-SAs@NC (SAs and NC refers to single atoms and N-doped carbon, respectively) also produced by pyrolysis, of bimetallic Co/Zn-ZIFs at 900 °C followed by further acid washing to remove the metal aggregates, shows a peak power density of about 105 mW cm^{-2}.[42] The ZIF-67@Pt/CB based batteries, two in a series connection, can power a light emitting diode (LED) (Figure 4c). As shown in Figure 4d, the ZIF-67@Pt/CB battery can operate with a small voltage window (i.e., the difference between charge and discharge voltage; 1.97 – 1.30 V) of ≤0.7 V, initially. This gives a round-trip efficiency of 65.9%, indicating a more efficient rechargeability (Figure 4e). It is interesting to note that battery can cycle with stable discharge and charge platforms at 1.28 V and 1.96 V, respectively, and remains stable in an extended cyclic test. For a measured period of 50 h (for 300 cycles), the battery shows a slight increase of roundtrip voltage window to 0.91 V. However, the Pt/CB based battery quickly deteriorates and the voltage window increases from 0.81 V to 1.35 V after just 50 cycles, indicating a poor rechargeability. The Pt/CB+IrO_2 catalyst based battery also shows an increased roundtrip voltage to 1.01 V within 180 cycles (Figure 4e).

Such a characteristic performance difference is attributed to a better OER activity for the ZIF-67@Pt/CB relative to Pt/CB, as demonstrated in Figure 2b,e. Note that OER is a more difficult reaction, with a higher reaction barrier.[28] Poor OER activity of Pt/CB means it require a high voltage for charging battery. The charge-/discharge voltage levels of zinc-air battery directly depend on the OER/ORR activity of the catalyst. The smallest possible potential difference between OER and ORR is an indication for a good bifunctional catalyst. This directly informs that zinc-air battery can be operated with smaller charge/discharge voltage window. This in turn can minimize the electrochemically induced deactivation of catalyst thus prolonging the battery cycle life. In the case of water oxidation or OER process the oxidation of electrode

materials is a common problem as it is carried out at a much higher positive potential, which falls in oxidation region, than the ORR. As shown in Figure 2, the ZIF-67 sample without Pt/CB exhibits relatively poor bifunctional activity thus requiring excess voltage at both OER - charge and ORR - discharge steps. Similarly, Pt/CB based battery also operates at higher positive voltage. Therefore, upon repeated cycling at such high positive voltages the electrolysis/oxidation of aqueous electrolyte can occur and generate very active oxygen species, decompose and more resistive.[43] This ultimately results in side reactions, such as oxidation of the carbon electrode (carbon corrosion), which will have a detrimental effect on ORR activity. Thus, upon repeated cycling, reactions will become more sluggish due to increased resistance and dissolution of oxidized carbon in Pt/CB air electrode. This is a main reason the Pt/CB based catalysts show poor cyclic stability as it is operated with relatively high positive voltage window compared to ZIF-67@Pt/CB catalyst (Figure 4d).

Here worth noting that ZIF-67@Pt/CB based battery also presented a good cycling durability when tested at

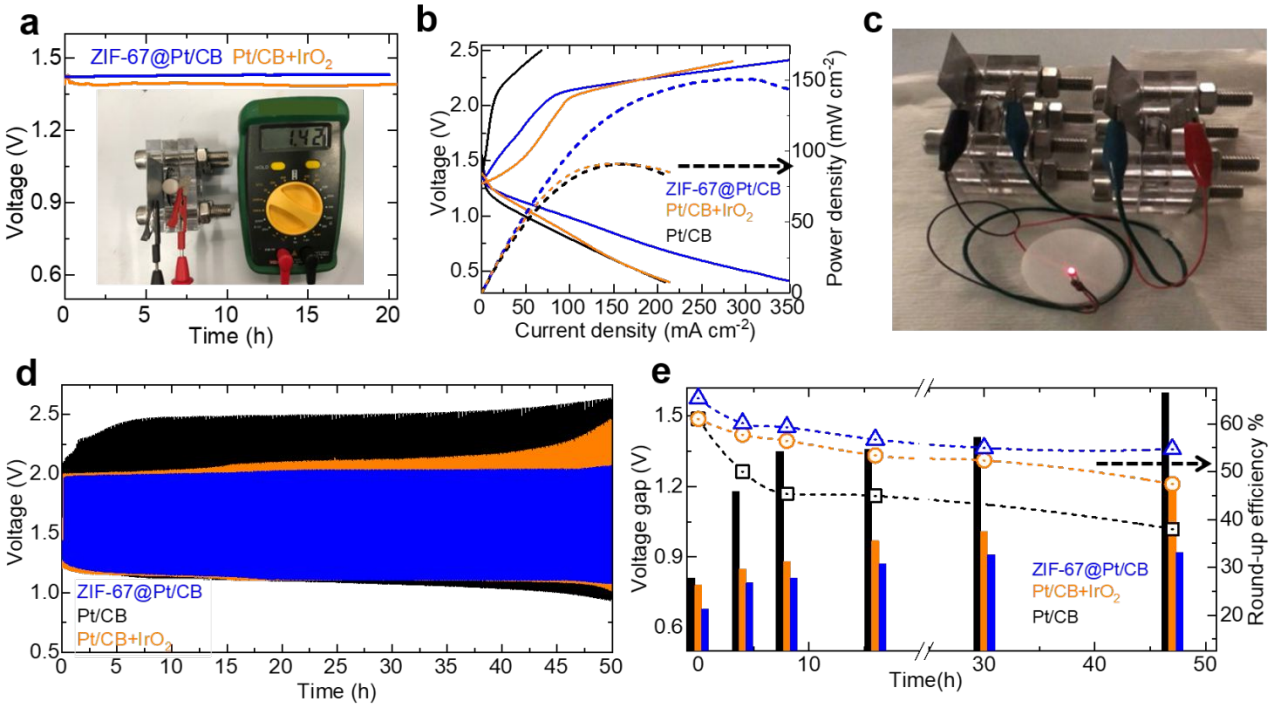

Figure 4. Rechargeable zinc-air battery performance characteristics of ZIF-67@Pt/CB with reference Pt/CB and Pt/CB+IrO_2 catalysts: a) OCV, recorded for 20 h, with inset photograph of assembled battery test cell. **b)** Charge-discharge polarization curves and corresponding discharge power density curves. **c)** Photograph showing the illuminating LED from two ZIF-67@Pt/CB based batteries connected in a series. **d)** Long-life charge-discharge cyclic tests of the batteries, operated at a fixed current density of 5 mA cm^{-2} (10 min for each cycle). **e)** Bar and line symbol graph describe the voltage gap and round-up efficiency of catalysts.

higher current densities of 10 and 20 mA cm^{-2} for 100 and 70 h, respectively (Figure S10 and S11). It further shows a superior discharge profiles at various current densities (Figure S12). Importantly, at reduced Pt/CB loading, a significantly improved activity durability of ZIF-67@Pt/CB-2, in a 2:1 mass ratio of ZIF-67 and Pt/CB; i.e., 25 wt% of Pt/CB loading compared to Pt/CB sample (Figure S13). All these emphasize the superior durability of ZIF-67@Pt/CB compared to reported bifunctional catalysts, summarised in Tables S3 and S4. In addition, the durable OER and ORR activities of catalysts also contribute to substantially improving cyclic stability of battery. For instance, as shown in Figure 5, the ZIF-67@Pt/CB sample exhibits a significantly improved ORR stability with an activity drop of ~15%, compared to ~48% in Pt/CB after 20 h of chronoamperometry test. But, ZIF-8@Pt/CB sample shows rapid activity degradation to ~56%, which is worse than Pt/CB. Here it is worth noting that ZIF-67@Pt/CB still maintain ~62% of its performance for an extended period of 85 h test, and still higher than the Pt/CB activity at 20 h (Figure S14). Similarly, ZIF-67@Pt/CB sample also exhibits high OER activity durability with retention of ~82% after 10 h (Figure 5b).

In order to understand such an impressive activity and durability performance, ZIF-67@Pt/CB sample used for ORR durability and battery cycling tests is further examined by SEM, TEM, XRD, FTIR and XPS (Figure 5c-j, and Figure S15-17). The SEM images after ORR durability test, for 20 h, show a partial decomposition of the ZIF-67 structure. TEM micrographs evidence development of a

sheet-like morphology at the expense of ZIF-67 polyhedron structure. XRD profiles show the transformation of crystalline ZIF-67 to an amorphous phase. FTIR spectra further confirm the ZIF-67 framework collapse and new cobalt-hydroxide phase formation. All these support for a formation of amorphous $Co(OH)_2$ nanosheets from in-situ degradation of ZIF-67 structure.[34,44-47] XPS spectra closely reveal new structure development and interaction between cobalt-related nanophase and platinum nanoparticles (Figure 5h-j). For instance, a shift in the Co 2p peak to lower binding energy is seen in a sample after ORR durability test compared to initial ZIF-67@Pt/CB. Diminished intensity of the satellite peak at about 786 eV, which is attributed to the Co^{2+} oxidation state in ZIF-67, indicates the increased concentration of Co^{3+} by formation of amorphous cobalt-hydroxide phase at the expense of Co-N coordination.[24,34,44-47] Deconvolution of Co $2p_{1/2}$ and Co $2p_{3/2}$ peaks confirms existence of Co^{2+} (peaks at ~798 and 781.2 eV) and Co^{3+} (peaks at ~795.5 and ~779.9 eV).[33,34,36-38,48] This is also evidenced in O 1s spectra, which show three peaks at 532.3, 531.5 and 530.4 eV, corresponding to adsorbed water (H_2O), hydroxy oxygen (O_H) and metal-O, respectively. This indicates interfacial interaction of platinum nanoparticles with cobalt-related hydroxide nanophase.[11,45] Here, it is worth noting formation of Co^{3+} from Co^{2+} without Pt oxidation. This can be attributed to already active Co^{2+} cation in ZIF-67 which is susceptible to oxidize easily to form Co^{3+} with a partial decomposition of ZIF-67 structure than oxidizing metallic Pt^0 under mild ORR negative potential.[33,34,36-38,48] This combination leads to an improved ORR durability (Figure 5a). Another interesting feature of ZIF-67@Pt/CB, a remarkable cycling stability in zinc-air battery

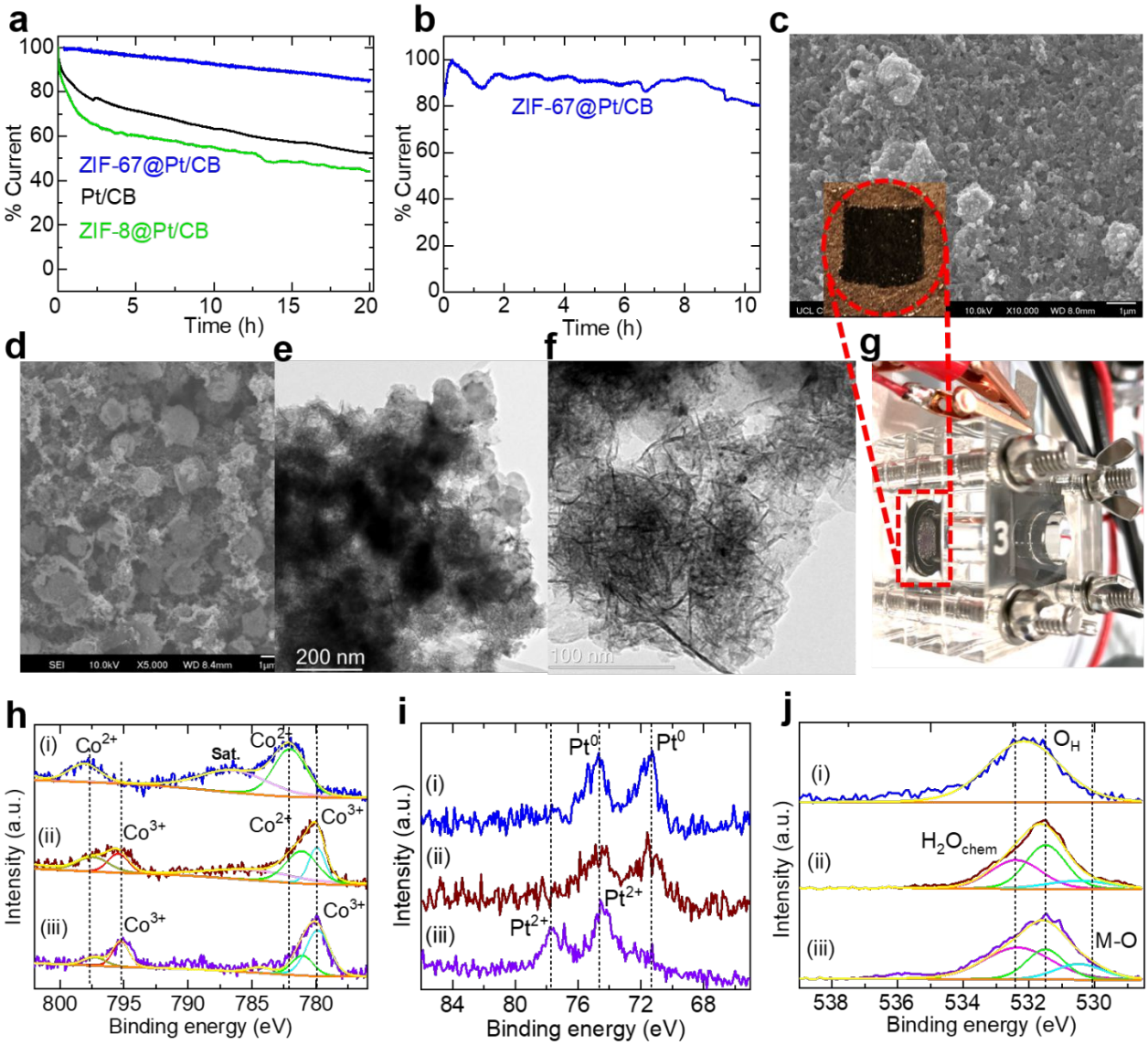

Figure 5. Catalytic activity durability and post electrochemical structural analysis of ZIF-67@Pt/CB catalyst: a) ORR chronoamperometric stability curves, recorded at 0.65 V (vs RHE) for 20 h, for comparison ZIF-8@Pt/CB and Pt/CB data is also recorded. **b)** OER chronopotentiometry curve, recorded at 10 mA cm^{-2} after conditioning for 15 min. **c,d)** SEM micrographs of samples after battery cycling (c) and ORR durability (d) tests conducted for 50 and 20 h, respectively. **e,f)**

TEM micrographs after ORR durability test for 20 h. **g)** Photograph of battery cell. **h-j)** Comparative XPS core level spectra of Co 2p, Pt 4f and O 1s obtained on the samples before (i), and after ORR durability for 20 h (ii) and battery cycling for 50 h (iii) tests. The relative peak shifts with exact positions are assigned to Co^{2+} (peaks at ~798 and 781.2 eV); Co^{3+} (peaks at ~795.3 and ~779.9 eV); Pt^0 at ~71.4 and 74.7 eV; Pt^{4+} at ~77.6 eV; Adsorbed water (H_2O) at ~532.3 eV; hydroxy oxygen (O_H) at ~531.5 eV; metal-oxygen at ~530.4 eV.

can be attributed to electrochemically induced in-situ formation of cobalt-oxyhydroxide/platinum-oxide nanophase. This is evidenced in XPS analysis of post-cycled catalyst sample collected from battery cathode after 50 h or 300 charge-discharge cycles (Figure 5c, g-j). Comparative XPS spectra of samples before and after ORR durability and battery cycling tests indicate increased degree of oxidation of cobalt and platinum. For instance, Co 2p XPS spectrum with a significantly increased Co^{3+}/Co^{2+} ratio is in good agreement with CoOOH phase.[46,49-52] The $CoOOH/PtO_2$ formation is also supported by Pt 4f and O 1s XPS spectra.[49,50] Earlier studies have shown that formation of CoOOH nanophase facilitate efficient OER activity, and therefore boost battery performance with prolonged cycle life.[46,51,52] SEM images recorded from the catalyst collected at different periods of zinc-air battery cycling test shows gradual decomposition of ZIF-67 structure to amorphous phase (Figure S17). Overall, the direct electrochemically induced in-situ formation of OER active CoOOH nanophase from degradation of ZIF-67 and its interfacial interaction with ORR active platinum nanoparticles result in highly efficient bifunctional electrocatalyst for zinc-air battery. Here, it is worth noting that ZIFs can be readily synthesized and used directly for electrochemical catalytic applications without subjecting them to extensive chemical manipulation, for example high temperature calcination or carbonization, as often reported in the literature. Overall, the results suggest that ZIF-67 is a promising and inexpensive catalyst material for the both ORR and OER, and applicable in rechargeable metal-air batteries. Such activities can be further improved by tailoring framework structures by the strategic design of MOFs/ZIFs hybrid nano/micro structures to enhance the surface/interface accessibility.

Conclusion

We have demonstrated a direct applicability of ZIF-67, one of the readily synthesized MOF structures at room temperature and/or commercially available MOFs, in rechargeable zinc-air battery for the first time. Here it is worth noting that no further post-synthesis chemical modifications, such as calcination or carbonization of ZIF-67 at high temperature is performed as most of the literature report MOF/ZIF based sacrificial templates route to produce carbon or metal-oxide/alloy based nanostructures. We discover a surprisingly active bifunctional performance for OER and ORR in a composite sample prepared from a cobalt-based ZIF and a platinum carbon black in 1:1 mass ratio (ZIF-67@Pt/CB) via facile solution mixing at room temperature. The sample shows a promising bifunctional activity, with a small potential difference of ~0.87 V compared to ZIF-8, ZIF-67 and Pt/CB. Interestingly, ZIF-67@Pt/CB enhances OER/ORR activity durability, for instance, ORR activity retention of about 85% compared to 52% in Pt/CB is observed for 20 h long chronoamperometry test. The isostructural ZIF-8@Pt/CB system shows poor activities. ZIF-67@Pt/CB based rechargeable zinc-air batteries delivers a remarkable performance with an excellent long term stability during 50 h cycling test and a peak power density of 150 mW cm^{-2} at high current density of 300 mA cm^{-2}. Such activities are attributed to the synergistic coupling between platinum nanoparticles and electrochemically induced in-situ formation of cobalt-oxyhydroxide nanophase from the self-degradation of ZIF-67 structure. The present study provides a straightforward and energy-efficient synthesis strategy for designing bifunctional electrocatalysts to develop a commercially feasible zinc-air battery technology.

Supporting Information. Preparation and characterization methods with additional experimental results and literature data comparisons is provided. This material is available free of charge via the Internet at http://pubs.acs.org.

AUTHOR INFORMATION

Corresponding Author

Srinivas Gadipelli - Electrochemical Innovation Lab, Department of Chemical Engineering, University College London, London, WC1E 7JE, United Kingdom.
Email: s.gadipelli@ucl.ac.uk

Funding Sources

This work was supported by the EPSRC (EP/R023581/1; EP/S018204/2; EP/P009050/1; EP/N032888/1; EP/M009394/1)

ACKNOWLEDGMENT

Brett and Shearing acknowledge the Faraday Institution for supporting energy storage research in the Electrochemical Innovation Lab (549585, 547601) and Shearing the Royal Academy of Engineering.

REFERENCES

(1) Zhou, T.; Zhang, N.; Wu, C.; Xie, Y. Surface/Interface Nanoengineering for Rechargeable Zn–Air Batteries. *Energy Environ. Sci.* **2020**, *13*, 1132–1153.
(2) Zhang, J.; Zhou, Q.; Tang, Y.; Zhang, L.; Li, Y. Zinc-Air Batteries: Are They Ready for Prime Time? *Chem. Sci.* **2019**, *10*, 8924–8929.
(3) Fu, J.; Liang, R.; Liu, G.; Yu, A.; Bai, Z.; Yang, L.; Chen, Z. Recent Progress in Electrically Rechargeable Zinc–Air Batteries. *Adv. Mater.* **2019**, *31*, 1805230.
(4) Yuan, Y.; Wang, J.; Adimi, S.; Shen, H.; Thomas, T.; Ma, R.; Attfield, J. P.; Yang, M. Zirconium Nitride Catalysts Surpass Platinum for Oxygen Reduction. *Nat. Mater.* **2020**, *19*, 282–286.
(5) Luo, M.; Zhao, Z.; Zhang, Y.; Sun, Y.; Xing, Y.; Lv, F.; Yang, Y.; Zhang, X.; Hwang, S.; Qin, Y.; Ma, J. Y.; Lin, F.; Su, D.; Lu, G.; Guo, S. PdMo Bimetallene for Oxygen Reduction Catalysis. *Nature* **2019**, *574*, 81–85.
(6) Zhang, L.; Doyle-Davis, K.; Sun, X. Pt-Based Electrocatalysts with High Atom Utilization Efficiency: From Nanostructures to Single Atoms. *Energy Environ. Sci.* **2019**, *12*, 492–517.

(7) Zeng, K.; Zheng, X.; Li, C.; Yan, J.; Tian, J.; Jin, C.; Strasser, P.; Yang, R. Recent Advances in Non-Noble Bifunctional Oxygen Electrocatalysts toward Large-Scale Production. *Adv. Funct. Mater.* **2020**, 27, 2000503.

(8) Wang, H. F.; Chen, L.; Pang, H.; Kaskel, S.; Xu, Q. MOF-Derived Electrocatalysts for Oxygen Reduction, Oxygen Evolution and Hydrogen Evolution Reactions. *Chem. Soc. Rev.* **2020**, *49*, 1414–1448.

(9) Huang, Y.; Wang, Y.; Tang, C.; Wang, J.; Zhang, Q.; Wang, Y.; Zhang, J. Atomic Modulation and Structure Design of Carbons for Bifunctional Electrocatalysis in Metal–Air Batteries. *Adv. Mater.* **2019**, *31*, 1803800.

(10) Kong, L.; Zhong, M.; Shuang, W.; Xu, Y.; Bu, X.-H. Electrochemically Active Sites inside Crystalline Porous Materials for Energy Storage and Conversion. *Chem. Soc. Rev.* **2020**, *49*, 2378–2407.

(11) Li, Z.; Niu, W.; Yang, Z.; Zaman, N.; Samarakoon, W.; Wang, M.; Kara, A.; Lucero, M.; Vyas, M. V.; Cao, H.; Zhou, H.; Sterbinsky, G. E.; Feng, Z.; Du, Y.; Yang, Y. Stabilizing Atomic Pt with Trapped Interstitial F in Alloyed PtCo Nanosheets for High-Performance Zinc-Air Batteries. *Energy Environ. Sci.* **2020**, *13*, 884–895.

(12) Li, G.; Zhao, S.; Zhang, Y.; Tang, Z. Metal – Organic Frameworks Encapsulating Active Nanoparticles as Emerging Composites for Catalysis : Recent Progress and Perspectives. **2018**, *1800702*, 1–43.

(13) Yang, Q.; Xu, Q.; Jiang, H. L. Metal-Organic Frameworks Meet Metal Nanoparticles: Synergistic Effect for Enhanced Catalysis. *Chem. Soc. Rev.* **2017**, *46*, 4774–4808.

(14) Gadipelli, S.; Li, Z.; Lu, Y.; Li, J.; Guo, J.; Skipper, N. T.; Shearing, P. R.; Brett, D. J. L. Size-Related Electrochemical Performance in Active Carbon Nanostructures: A MOFs-Derived Carbons Case Study. *Adv. Sci.* **2019**, *6*, 1901517.

(15) Cai, Z.; Wang, Z.; Kim, J.; Yamauchi, Y. Hollow Functional Materials Derived from Metal–Organic Frameworks: Synthetic Strategies, Conversion Mechanisms, and Electrochemical Applications. *Adv. Mater.* **2019**, *31*, 1804903.

(16) Sun, H.; Zhu, J.; Baumann, D.; Peng, L.; Xu, Y.; Shakir, I.; Huang, Y.; Duan, X. Hierarchical 3D Electrodes for Electrochemical Energy Storage. *Nature Reviews Materials*. Springer US **2019**, 4, 45–60.

(17) Zhu, J.; Xiao, M.; Li, G.; Li, S.; Zhang, J.; Liu, G.; Ma, L.; Wu, T.; Lu, J.; Yu, A.; Su, D.; Jin, H.; Wang, S.; Chen, Z. A Triphasic Bifunctional Oxygen Electrocatalyst with Tunable and Synergetic Interfacial Structure for Rechargeable Zn-Air Batteries. *Adv. Energy Mater.* **2020**, *10*, 1903003.

(18) Xiao, X.; Zou, L.; Pang, H.; Xu, Q. Synthesis of Micro/Nanoscaled Metal-Organic Frameworks and Their Direct Electrochemical Applications. *Chem. Soc. Rev.* **2020**, *49*, 301–331.

(19) Wang, Q.; Astruc, D. State of the Art and Prospects in Metal-Organic Framework (MOF)-Based and MOF-Derived Nanocatalysis. *Chem. Rev.* **2020**, *120*, 1438–1511.

(20) Gadipelli, S.; Howard, C. A.; Guo, J.; Skipper, N. T.; Zhang, H.; Shearing, P. R.; Brett, D. J. L. Superior Multifunctional Activity of Nanoporous Carbons with Widely Tunable Porosity: Enhanced Storage Capacities for Carbon-Dioxide, Hydrogen, Water, and Electric Charge. *Adv. Energy Mater.* **2020**, *10*, 1903649.

(21) Hanikel, N.; Prévot, M. S.; Yaghi, O. M. MOF Water Harvesters. *Nat. Nanotechnol.* **2020**, *15*, 348–355.

(22) Zhang, K.; Kirlikovali, K. O.; Le, Q. Van; Jin, Z.; Varma, R. S.; Jang, H. W.; Farha, O. K.; Shokouhimehr, M. Extended Metal–Organic Frameworks on Diverse Supports as Electrode Nanomaterials for Electrochemical Energy Storage. *ACS Appl. Nano Mater.* **2020**, *3*, 3964–3990.

(23) Ding, M.; Flaig, R. W.; Jiang, H. L.; Yaghi, O. M. Carbon Capture and Conversion Using Metal-Organic Frameworks and MOF-Based Materials. *Chem. Soc. Rev.* **2019**, *48*, 2783–2828.

(24) Gadipelli, S.; Zhao, T.; Shevlin, S. A.; Guo, Z. Switching Effective Oxygen Reduction and Evolution Performance by Controlled Graphitization of a Cobalt–Nitrogen–Carbon Framework System. *Energy Environ. Sci.* **2016**, *9*, 1661–1667.

(25) Srinivas, G.; Krungleviciute, V.; Guo, Z. X.; Yildirim, T. Exceptional CO_2 Capture in a Hierarchically Porous Carbon with Simultaneous High Surface Area and Pore Volume. *Energy Environ. Sci.* **2014**, *7*, 335–342.

(26) Gadipelli, S.; Guo, Z. X. Tuning of ZIF-Derived Carbon with High Activity, Nitrogen Functionality, and Yield - A Case for Superior CO_2 Capture. *ChemSusChem* **2015**, *8*, 2123–2132.

(27) Hao, J.; Babu, D. J.; Liu, Q.; Chi, H.-Y.; Lu, C.; Liu, Y.; Agrawal, K. V. Synthesis of High-Performance Polycrystalline Metal–Organic Framework Membranes at Room Temperature in a Few Minutes. *J. Mater. Chem. A* **2020**, *8*, 7633–7640.

(28) Rubio-Martinez, M.; Avci-Camur, C.; Thornton, A. W.; Imaz, I.; Maspoch, D.; Hill, M. R. New Synthetic Routes towards MOF Production at Scale. *Chemical Society Reviews*. Royal Society of Chemistry 2017, *11*, 3453–3480.

(29) Talin, A. A.; Centrone, A.; Ford, A. C.; Foster, M. E.; Stavila, V.; Haney, P.; Kinney, R. A.; Szalai, V.; El Gabaly, F.; Yoon, H. P.; Léonard, F.; Allendorf, M. D. Tunable Electrical Conductivity in Metal-Organic Framework Thin-Film Devices. *Science.* **2014**, *343*, 66–69.

(30) Ellis, J. E.; Zeng, Z.; Hwang, S. I.; Li, S.; Luo, T.-Y.; Burkert, S. C.; White, D. L.; Rosi, N. L.; Gassensmith, J. J.; Star, A. Growth of ZIF-8 on Molecularly Ordered 2-Methylimidazole/Single-Walled Carbon Nanotubes to Form Highly Porous, Electrically Conductive Composites. *Chem. Sci.* **2019**, *10*, 737–742.

(31) Zhang, W.; Shi, W.; Ji, W.; Wu, H.; Gu, Z.; Wang, P.; Li, X.; Qin, P.; Zhang, J.; Fan, Y.; Wu, T.; Fu, Y.; Zhang, W.; Huo, F. Microenvironment of MOF Channel Coordination with Pt NPs for Selective Hydrogenation of Unsaturated Aldehydes. *ACS Catal.* **2020**, *10*, 5805–5813.

(32) Gadipelli, S.; Travis, W.; Zhou, W.; Guo, Z. A Thermally Derived and Optimized Structure from ZIF-8 with Giant Enhancement in CO_2 uptake. *Energy Environ. Sci.* **2014**, *7*, 2232–2238.

(33) He, W.; Ifraemov, R.; Raslin, A.; Hod, I. Room-Temperature Electrochemical Conversion of Metal – Organic Frameworks into Porous Amorphous Metal Sulfides with Tailored Composition and Hydrogen Evolution Activity. **2018**, *18*, 1707244.

(34) Zheng, W.; Liu, M.; Lee, L. Y. S. Electrochemical Instability of Metal–Organic Frameworks: In Situ Spectroelectrochemical Investigation of the Real Active Sites. *ACS Catal.* **2020**, *10*, 81–92.

(35) Tao, L.; Lin, C. Y.; Dou, S.; Feng, S.; Chen, D.; Liu, D.; Huo, J.; Xia, Z.; Wang, S. Creating Coordinatively Unsaturated Metal Sites in Metal-Organic-Frameworks as Efficient Electrocatalysts for the Oxygen Evolution Reaction: Insights into the Active Centers. *Nano Energy* **2017**, *41*, 417–425.

(36) Dou, S.; Dong, C.-L.; Hu, Z.; Huang, Y.-C.; Chen, J.; Tao, L.; Yan, D.; Chen, D.; Shen, S.; Chou, S.; Wang, S. Atomic-Scale CoO_x Species in Metal-Organic Frameworks for Oxygen Evolution Reaction. *Adv. Funct. Mater.* **2017**, *27*, 1702546.

(37) Jia, G.; Liu, L.; Zhang, L.; Zhang, D.; Wang, Y.; Cui, X.; Zheng, W. 1D Alignment of ZnO@ZIF-8/67 Nanorod Arrays for Visible-Light-Driven Photoelectrochemical Water Splitting. *Appl. Surf. Sci.* **2018**, *448*, 254–260.

(38) Wu, C.; Guo, J.; Zhang, J.; Zhao, Y.; Tian, J.; Isimjan, T. T.; Yang, X. Palladium Nanoclusters Decorated Partially Decomposed Porous ZIF-67 Polyhedron with Ultrahigh Catalytic Activity and Stability on Hydrogen Generation. *Renew. Energy* **2019**, *136*, 1064–1070.

(39) Guo, J.; Gadipelli, S.; Yang, Y.; Li, Z.; Lu, Y.; Brett, D. J. L.; Guo, Z. An Efficient Carbon-Based ORR Catalyst from Low-Temperature Etching of ZIF-67 with Ultra-Small Cobalt Nanoparticles and High Yield. *J. Mater. Chem. A* **2019**, *7*, 3544–3551.

(40) Zhong, Y.; Pan, Z.; Wang, X.; Yang, J.; Qiu, Y.; Xu, S.; Lu, Y.; Huang, Q.; Li, W. Hierarchical Co_3O_4 Nano-Micro Arrays Featuring Superior Activity as Cathode in a Flexible and Rechargeable Zinc–Air Battery. *Adv. Sci.* **2019**,*6* , 1802243.

(41) Xu, Y.; Deng, P.; Chen, G.; Chen, J.; Yan, Y.; Qi, K.; Liu, H.; Xia, B. Y. 2D Nitrogen-Doped Carbon Nanotubes/Graphene Hybrid as Bifunctional Oxygen Electrocatalyst for Long-Life

Rechargeable Zn–Air Batteries. *Adv. Funct. Mater.* **2020**, *30*, 1906081.

(42) Han, X.; Ling, X.; Wang, Y.; Ma, T.; Zhong, C.; Hu, W.; Deng, Y. Generation of Nanoparticle, Atomic-Cluster, and Single-Atom Cobalt Catalysts from Zeolitic Imidazole Frameworks by Spatial Isolation and Their Use in Zinc–Air Batteries. *Angew. Chem* **2019**, *16*, 5413–5418.

(43) Pei, P.; Wang, K.; Ma, Z. Technologies for Extending Zinc-Air Battery's Cyclelife: A Review. *Appl. Energy* **2014**, *128*, 315–324.

(44) Wang, K.; Wu, W.; Tang, Z.; Li, L.; Chen, S.; Bedford, N. M. Hierarchically Structured $Co(OH)_2$/CoPt/N-CN Air Cathodes for Rechargeable Zinc-Air Batteries. *ACS Appl. Mater. Interfaces* **2019**, *11*, 4983–4994.

(45) Kong, F.; Zhang, W.; Sun, L.; Huo, L.; Zhao, H. Interface Electronic Coupling in Hierarchical FeLDH(FeCo)/$Co(OH)_2$ Arrays for Efficient Electrocatalytic Oxygen Evolution. *ChemSusChem* **2019**, *12*, 3592–3601.

(46) Zhou, J.; Wang, Y.; Su, X.; Gu, S.; Liu, R.; Huang, Y.; Yan, S.; Li, J.; Zhang, S. Electrochemically Accessing Ultrathin Co (Oxy)-Hydroxide Nanosheets and Operando Identifying Their Active Phase for the Oxygen Evolution Reaction. *Energy Environ. Sci.* **2019**, *12*, 739–746.

(47) Zha, Q.; Xu, W.; Li, X.; Ni, Y. Chlorine-Doped α-$Co(OH)_2$ Hollow Nano-Dodecahedrons Prepared by a ZIF-67 Self-Sacrificing Template Route and Enhanced OER Catalytic Activity. *Dalt. Trans.* **2019**, *48*, 12127–12136.

(48) Li, S.; Peng, S.; Huang, L.; Cui, X.; Al-Enizi, A. M.; Zheng, G. Carbon-Coated Co^{3+}-Rich Cobalt Selenide Derived from ZIF-67 for Efficient Electrochemical Water Oxidation. *ACS Appl. Mater. Interfaces* **2016**, *8*, 20534–20539.

(49) Wang, Z.; Ren, X.; Shi, X.; Asiri, A. M.; Wang, L.; Li, X.; Sun, X.; Zhang, Q.; Wang, H. A Platinum Oxide Decorated Amorphous Cobalt Oxide Hydroxide Nanosheet Array towards Alkaline Hydrogen Evolution. *J. Mater. Chem. A* **2018**, *6*, 3864–3868.

(50) Mom, R.; Frevel, L.; Velasco-Vélez, J.-J.; Plodinec, M.; Knop-Gericke, A.; Schlögl, R. The Oxidation of Platinum under Wet Conditions Observed by Electrochemical X-Ray Photoelectron Spectroscopy. *J. Am. Chem. Soc.* **2019**, *141*, 6537–6544.

(51) Huang, J.; Chen, J.; Yao, T.; He, J.; Jiang, S.; Sun, Z.; Liu, Q.; Cheng, W.; Hu, F.; Jiang, Y.; Pan, Z.; Wei, S. CoOOH Nanosheets with High Mass Activity for Water Oxidation. *Angew. Chem. Int. Ed.* **2015**, *54*, 8722–8727.

(52) Huang, Z.-F.; Song, J.; Du, Y.; Xi, S.; Dou, S.; Nsanzimana, J. M. V.; Wang, C.; Xu, Z. J.; Wang, X. Chemical and Structural Origin of Lattice Oxygen Oxidation in Co–Zn Oxyhydroxide Oxygen Evolution Electrocatalysts. *Nat. Energy* **2019**, *4*, 329–338.

Insert Table of Contents artwork here